







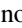
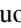
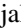









In-beam γ -ray spectroscopy of $^{211,213}\text{Ac}$ and ^{211}Ra

J. Louko ^{1,*}, K. Auranen ¹, J. Uusitalo ¹, A. D. Briscoe ^{1,†}, T. Grahn ¹, P. T. Greenlees ¹, A. Illana ^{1,‡}, H. Joukainen ¹,
R. Julin ¹, H. Jutila ¹, M. Leino ¹, M. Luoma ¹, J. Ojala ¹, J. Pakarinen ¹, A. Raggio ¹, P. Rahkila ¹,
J. Romero ^{1,2}, P. Ruotsalainen ¹, M. Sandzelius ¹, J. Sarén ¹, A. Tolosa-Delgado ^{1,§} and G. Zimba ^{1,||}

¹Accelerator Laboratory, Department of Physics, University of Jyväskylä, FI-40014 Jyväskylä, Finland

²University of Liverpool, Department of Physics, Oliver Lodge Laboratory, Liverpool L69 7ZE, United Kingdom



(Received 10 May 2024; accepted 28 August 2024; published 11 September 2024)

The first in-beam γ -ray spectroscopic study of the neutron-deficient actinium isotopes $^{211,213}\text{Ac}$ has been carried out at the Accelerator Laboratory of the University of Jyväskylä using a highly selective recoil-decay tagging method with the JUROGAM 3 germanium-detector array and MARA separator. The nuclei of interest were produced using the $^{175}\text{Lu}(^{40}\text{Ar}, 4n)^{211}\text{Ac}$ and $^{180}\text{Hf}(^{37}\text{Cl}, 4n)^{213}\text{Ac}$ fusion-evaporation reactions. Excited states in ^{211}Ac were observed for the first time. In ^{211}Ac and ^{213}Ac low-lying core-excited states whose excitation energies follow the systematic trends of their respective core states in even-even isotones ^{210}Ra and ^{212}Ra were identified. Additionally, we were able to extend the level scheme of ^{211}Ra , which was also produced in the $^{40}\text{Ar} + ^{175}\text{Lu}$ reaction. We also remeasured the half-lives of the ground states of these nuclei and also that of the ($^{13/2}^+$) isomeric state of ^{211}Ra .

DOI: [10.1103/PhysRevC.110.034311](https://doi.org/10.1103/PhysRevC.110.034311)

I. INTRODUCTION

Extensive research of nuclear structure and shape evolution [1] in the $N < 126$, translead region has been ongoing for several decades at the Accelerator Laboratory of the University of Jyväskylä (JYFL-ACCLAB) and other laboratories. Early studies utilized, for example, α -decay spectroscopy, later extended by in-beam techniques. In the α -decay process, states with similar initial and final state structures are favored, which can indirectly provide information about the deformation of the initial state if the final state structure is known and vice versa [2]. Experiments employing in-gas laser ionization and spectroscopy techniques [3] have also confirmed results from the decay studies by measuring ground-state charge distributions and observed enlarged radii when the ground state becomes deformed.

In-beam γ -ray spectroscopy can be used to probe the developing shape change of nuclei before it is seen for the ground state. The information is gained by studying a range of nuclei and their level-energy systematics. In-beam γ -ray spectroscopy can also reveal shape coexistence of excited states by observing rotational bands based on different shapes [4].

Measurements of excited states provide a good benchmark for nuclear theories and give valuable input for further developments. In general, the shape evolution predicted by current mean-field models [5,6] in the region of interest of the present work is reproduced quite well. Once leaving the spherical $N = 126$ shell closure towards the proton drip line a shape change towards weak oblate deformation is predicted, and closer to the $N = 104$ neutron midshell a strong prolate deformation takes over. However, experimental confirmation becomes more challenging due to the decreasing production cross sections and short lifetimes when approaching the proton drip line.

Due to the experimental challenges, not much is known about the structure of odd-even actinium ($Z = 89$) isotopes in this region. Besides α -decay studies [7–11], only one in-gas laser spectroscopic study has been carried out [12]. No γ -ray transitions were known in ^{211}Ac and just five transitions were tentatively placed to the level scheme of ^{213}Ac in Ref. [9]. In the isotope ^{211}Ra , six γ -ray transitions were known [13–15], all of which reside below the ($^{13/2}^+$) isomeric state. The main motivation of this work was to continue studying this not yet so well-known area of the nuclear chart, and especially investigate low-lying excited states of actinium and radium isotopes and their level-energy systematics.

II. EXPERIMENTAL DETAILS

The nuclei of interest were produced using two different fusion-evaporation reactions, $^{40}\text{Ar} + ^{175}\text{Lu}$ and $^{37}\text{Cl} + ^{180}\text{Hf}$. Experimental production cross section for ^{211}Ac and ^{213}Ac were in the order of $50\ \mu\text{b}$ with beam energies of 182 and 170 MeV, respectively. While these were independent measurements, it later proved to be advantageous to do

*Contact author: jussi.i.louko@jyu.fi

[†]Present address: University of Liverpool, Department of Physics, Oliver Lodge Laboratory, Liverpool L69 7ZE, United Kingdom.

[‡]Present address: Grupo de Física Nuclear and IPARCOS, Universidad Complutense de Madrid, CEI Moncloa, E-28040 Madrid, Spain.

[§]Present address: European Organization for Nuclear Research (CERN), Geneva, Switzerland.

^{||}Present address: Facility for Rare Isotope Beams, Michigan State University, 640 South Shaw Lane, East Lansing, MI 48824, USA.

TABLE I. Beam and target summary.

Beam	$E_{\text{beam}}^{\text{lab}}$ (MeV)	I_{beam} (pnA)	Target	d_{target} ($\mu\text{g}/\text{cm}^2$)	Duration (h)
$^{40}\text{Ar}^{8+}$	182	14	$^{175}\text{Lu}^{\text{a}}$	930	55
$^{40}\text{Ar}^{8+}$	186	15	$^{175}\text{Lu}^{\text{a}}$	320	2
$^{40}\text{Ar}^{8+}$	182	20	$^{175}\text{Lu}^{\text{a}}$	320	44
$^{40}\text{Ar}^{8+}$	182	19	$^{175}\text{Lu}^{\text{a}}$	460	66
$^{37}\text{Cl}^{7+}$	170	10	$^{180}\text{Hf}^{\text{b}}$	180 ^c	126
$^{37}\text{Cl}^{7+}$	170	12	$^{\text{nat}}\text{Hf}^{\text{b}}$	500	16

^a47 $\mu\text{g}/\text{cm}^2$ carbon charge reset foil downstream from the target.

^b21 $\mu\text{g}/\text{cm}^2$ carbon charge reset foil downstream from the target.

^cEstimation, based on an α -particle energy-loss measurement.

cross-checking between these data sets to solve some ambiguities regarding the presence of neighboring isotopes. For more details regarding the beam and target combinations used, see Table I.

The beams were provided by the electron-cyclotron resonance ion source and the K130 cyclotron of JYFL-ACCLAB. The JUROGAM 3 germanium-detector array [16] was deployed for the detection of prompt γ rays at the target position. Stacked tin and copper absorbers of thicknesses 0.25 mm and 0.5 mm, respectively, were placed in front of the germanium detectors to decrease the x-ray yield. Reaction products of interest were separated from the unreacted primary beam and other unwanted particles using the MARA vacuum-mode mass separator [17,18], and they were subsequently identified at the focal plane using the highly selective recoil-decay tagging (RDT) method [19,20].

The MARA focal plane consisted of a multiwire proportional counter (MWPC) with 0.9- μm thick mylar foil windows, a 300- μm thick double-sided silicon-strip detector (DSSD), and 1-mm thick punch-through veto detectors. Three broad-energy germanium detectors, surrounding the focal-plane chamber, were used to detect γ rays after the de-excitation of directly populated long-lived isomeric states or after decays to excited states.

This instrumentation, combined with the triggerless total data readout data-acquisition system [21], makes it possible to

apply different gating conditions and use various correlation techniques during the offline analysis. For further details of typical setups and the other techniques used with MARA, see Ref. [22] and references therein.

III. RESULTS

During the analysis, an event is constructed around the DSSD data. If the given X and Y strip signals have a similar amplitude and time, an event is assigned to that quasipixel. This event can then have multiple attributes. For example, it can be classified as a fusion-recoil event based on its implantation energy and time of flight between the DSSD and the MWPC. Alternatively, it can be classified as a decay event, if its energy is in a suitable range and signals were not detected in the MWPC nor in the punch-through detectors. Otherwise, it is considered as another type of beam related event such as a scattered target- or beam-like particle or a lighter punch-through particle of unspecified origin and it can be ignored for the purpose of tagging correlations.

If there are subsequent recoil and decay events in the same DSSD pixel, they can be plotted in a tagging plot, as shown in Fig. 1. Once an event is tagged in this manner, temporal correlations can be made to prompt γ -ray events seen by the germanium detectors at the target position. After the transitions belonging to the nucleus of interest were identified, a

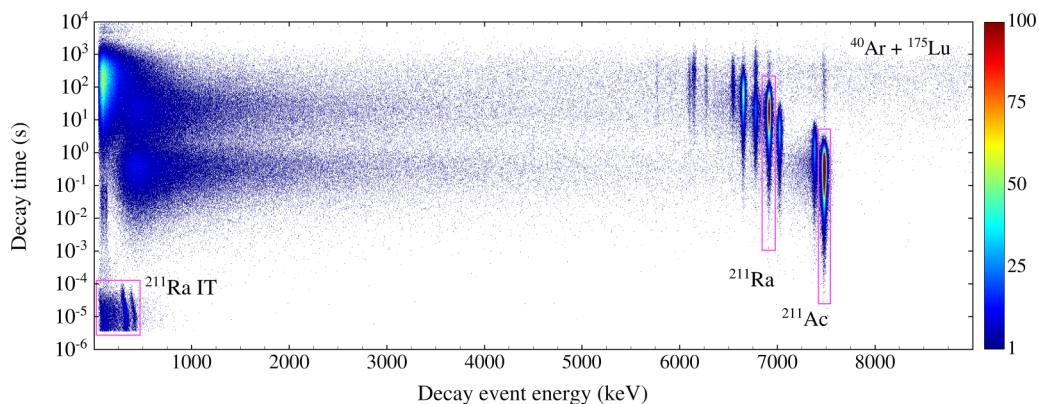


FIG. 1. Decay time as a function of the decay energy for the decay events following a recoil-implantation event in the same pixel of the DSSD. Three example gates are shown in pink, one for the internal conversion electrons from the ^{211}Ra isomeric 395 keV $M2$ transition (IT) and two for the α decays as indicated.

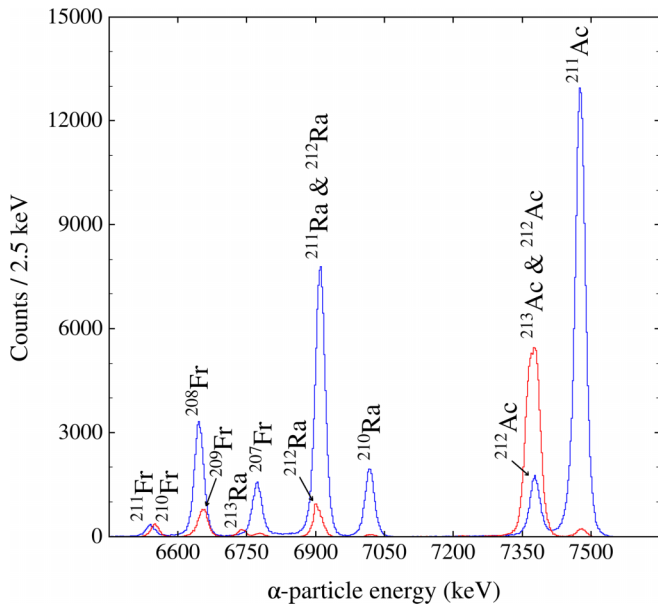


FIG. 2. Recoil-decay correlated α -particle energy spectra from reactions $^{40}\text{Ar} + ^{175}\text{Lu}$ (blue) and $^{37}\text{Cl} + ^{180}\text{Hf}$ (red).

level scheme could be constructed based on transition intensities, energy sums, and γ - γ coincidences.

A. Isotope ^{213}Ac

When studying the nucleus ^{213}Ac , the main contaminant was its neighbor, ^{212}Ac , produced in the $5n$ channel. The α -particle energy and half-life of these two nuclei are very similar, and even the decay properties of daughter nuclei are similar. However, the previously unknown transitions of ^{212}Ac were reliably identified through a cross-bombardment in the reaction $^{40}\text{Ar} + ^{175}\text{Lu}$. Energy spectra of α particles from these two reactions are shown in Fig. 2. The relative shifts in the yields of the products are apparent. The clean ^{212}Ac α -peak allowed us to distinguish the transitions belonging to it and ^{213}Ac , see blue histogram in Fig. 2. Origin of the transitions were also confirmed by separately setting gates on either side of the doublet α peak in the reaction $^{37}\text{Cl} + ^{180}\text{Hf}$. The lower energy side of the α peak enhanced the transitions of ^{213}Ac , while the higher energy side enhanced the transitions belonging to ^{212}Ac , which is consistent with the reported α -particle energies of ^{213}Ac and ^{212}Ac in the literature, 7360(6) keV and 7379(8) keV, respectively [23,24].

Two γ - γ coincidence spectra are shown in Fig. 3. The coincidence γ -ray energy spectrum with the gate set on the 613-keV ground-state transition in Fig. 3(a) shows all three other strong peaks present in the singles spectrum in Fig. 4(a) and additionally the peak at 1116 keV is also present. The 450-keV transition is also in coincidence with the 446-keV transition as seen in Fig. 3(b). In fact, the 613-keV, 821-keV, 450-keV, and 446-keV transitions are mutually coincident, suggesting their placement in one cascade.

The 613-keV, 821-keV, 450-keV transitions were also observed in the α -decay study of ^{217}Pa [9]. However, we were able to establish their correct sequence based on the in-beam γ -ray intensities. Spins and parities for 467-keV and 634-keV

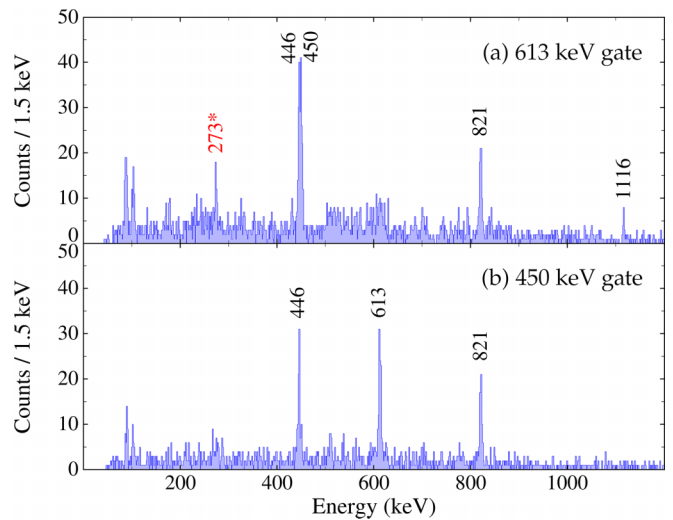


FIG. 3. ^{213}Ac α -decay tagged prompt coincidence γ -ray energy spectra gated on the (a) 613-keV and (b) 450-keV γ -ray transitions. The 273-keV transition marked in red (*) is from the contaminant ^{212}Ac .

states seen in the aforementioned α -decay study are suggested on the basis of the hindrance-factor systematics presented in Ref. [25]. The constructed level scheme is shown in Fig. 5. Not all transitions could be confidently placed on it. A list of all observed transitions and their relative intensities can be found in Table II. Spin and parity assignments and suggested configurations for selected states are discussed in Sec. IV.

The half-life of ^{213}Ac was determined from the 446-450-821-613-keV γ -gated recoil- α correlations, using the logarithmic time-scale method, described in Ref. [26]. The obtained result was 771(14) ms, which is in an agreement the reported literature value of 738(16) ms [27].

B. Isotope ^{212}Ac

Several transitions belonging to the isotope ^{212}Ac could be clearly seen with both reactions. The shell-model calculations in Ref. [3], suggest that the ground state should have a spin and parity of 7^+ , above which 6^+ and 5^+ states lie at around 200 keV of excitation energy. We observed several suitable transitions in this energy range, as is seen in the recoil- α gated γ -ray energy spectrum in Fig. 4(b). However, limited data did not allow for construction of the level scheme. A summary of the observed transitions and their prompt coincidences is presented in Table II. The half-life of ^{212}Ac was determined from the recoil- α correlations of the non- ^{213}Ac contaminated $^{40}\text{Ar} + ^{175}\text{Lu}$ dataset, using the logarithmic time-scale method [26]. The obtained result was 881(15) ms, which is in a good agreement with the half-life of 880(35) ms reported in Ref. [28].

C. Isotope ^{211}Ac

Identification of the transitions belonging to the ^{211}Ac nucleus was more straightforward as no strong overlapping activities were present. A recoil- α gated γ -ray energy spectrum is shown in Fig. 4(c).

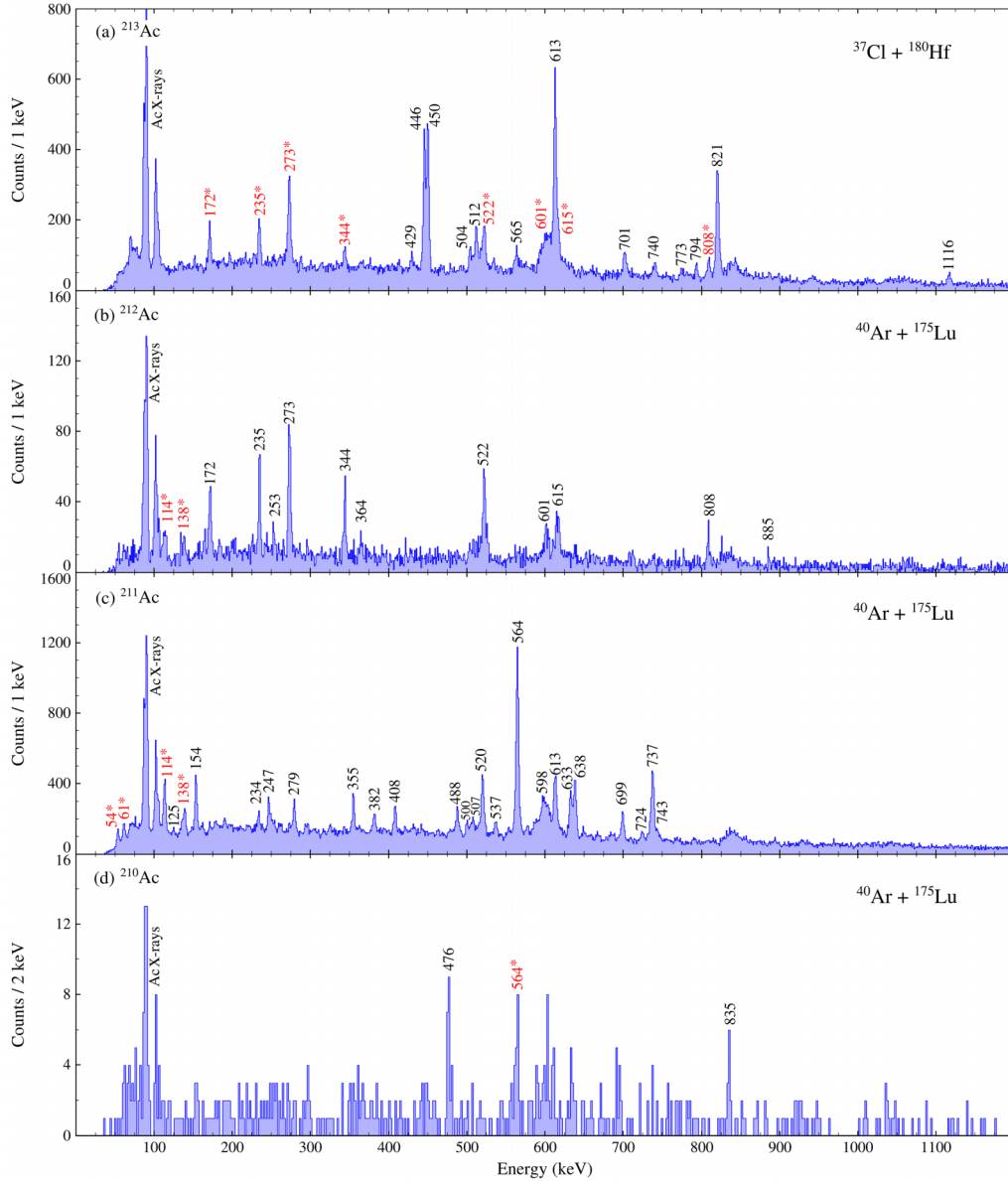


FIG. 4. (a) Recoil- α gated prompt γ -ray energy spectrum for ^{213}Ac . Transitions marked in red (*) belong to the contaminant of ^{212}Ac , as can be clearly seen by comparing it to the spectrum, shown in (b). (b) Recoil- α gated prompt γ -ray energy spectrum for ^{212}Ac . Transitions marked in red (*), originate from the target (^{175}Lu) due to beam induced Coulomb excitations. (c) Recoil- α gated prompt γ -ray energy spectrum for ^{211}Ac . Transitions marked in red (*) originate from Coulomb excitations of the ^{175}Lu target. (d) Prompt γ -ray energy spectrum for ^{210}Ac , which was obtained by applying a tight recoil- α - α gate, favoring the decay properties of ^{210}Ac . A contaminant line from ^{211}Ac is marked in red (*).

Selected γ -ray coincidence spectra are shown in Fig. 6. The spectrum in Fig. 6(a) shows the transitions placed above the proposed 564-keV ground state transition. Notably, the 488-613-keV cascade is missing and the 537-keV transition is present. Based on the energy sums and systematics, the 488-613-keV cascade is then assigned to feed the ground state in parallel with the 564-keV transition in a similar manner as in the neighboring odd-even isotone ^{209}Fr [29]. The 633-keV and 743-keV transitions seen in the spectra of Figs. 6(a) and 6(c) are placed to form an alternative decay path from the 1940 keV state to the 564 keV state. The 638-keV gated spectrum in Fig. 6(b) shows the main band

and the transition is also in a prompt coincidence with the 154-keV transition. However, in the 279-keV gated spectrum Fig. 6(c), the 154-keV transition is not present, suggesting its placement in parallel with the 279-keV transition. This placement is also supported by the observed 125-keV transition, in coincidence with the 154-keV transition, which completes the energy sum. Based on the energy sums and systematics as well as γ - γ coincidences and intensities, we were able to place 11 out of 22 transitions into the level scheme, shown in Fig. 7, and give tentative spin and parity assignments as well as configurations for the states. List of all observed transitions and their properties are given in Table II.

TABLE II. Properties of the transitions assigned to $^{210-213}\text{Ac}$ and ^{211}Ra . Relative γ -ray transition intensities ($I_{\gamma}^{\text{rel.}}$) are measured from the recoil- α -gated γ -ray singles spectra and corrected by the efficiency obtained using $^{152}\text{Eu} + ^{133}\text{Ba}$ mixed source. Spin and parity of the initial (I_i^{π}) and final states (I_f^{π}) and multipolarities (σL) are to be considered as tentative. For ^{212}Ac , prompt γ - γ coincidences are given. Reported errors are nominal 1σ interval and they include statistical uncertainties of the fittings as well as estimated experimental uncertainties associated with the Doppler correction and background.

Nucleus	E_{γ} (keV)	$I_{\gamma}^{\text{rel.}}$ (%)	I_i^{π}	I_f^{π}	σL
^{213}Ac	429.4(7)	8(1)			
	445.9(5)	60(5)	(23/2 ⁻)	(21/2 ⁻)	(M1 + E2)
	450.3(5)	74(5)	(21/2 ⁻)	(17/2 ⁻)	(E2)
	466.5(2) ^a		(7/2 ⁻)	9/2 ⁻	(M1 + E2)
	504.2(6)	17(2)			
	512.1(6) ^b	33(3)			
	565.3(8) ^b	16(3)			
	612.5(6)	100(8)	(13/2 ⁻)	9/2 ⁻	(E2)
	634.3(1) ^a		(11/2 ⁻)	9/2 ⁻	(M1 + E2)
	701.2(7) ^b	19(3)			
	740.4(9) ^b	12(3)			
	773.4(6) ^b	7(2)			
	793.7(6) ^b	14(2)			
	820.5(6)	80(8)	(17/2 ⁻)	(13/2 ⁻)	(E2)
	1115.7(6)	13(2)		(13/2 ⁻)	
Prompt γ - γ coincidences					
^{212}Ac	171.8(5)	34(6)	235.0, 273.2, 344.0, 364.3, 521.9		
	235.0(4)	47(7)	171.8, 273.2, 344.0, 521.9		
	252.9(5)	10(2)	273.2		
	273.2(5)	100(15)	171.8, 235.0, 252.9, 344.0, 521.9, 884.7		
	344.0(4)	44(7)	171.8, 235.0, 273.2, 521.9		
	364.3(5)	8(2)	171.8, 521.9		
	521.9(4)	84(13)	171.8, 235.0, 273.2, 344.0, 364.3, 808.3		
	601.3(6)	41(6)			
	615.2(5)	51(8)			
	808.3(4)	39(6)	521.9		
	884.7(6)	21(5)	273.2		
^{211}Ac	125.0(6)	5(1)	(23/2 ⁻)		
	153.8(6)	14(1)		(21/2 ⁻)	
	234.1(7) ^b	5(1)			
	246.9(6) ^b	7(1)			
	279.3(6)	9(1)	(23/2 ⁻)	(21/2 ⁻)	(M1 + E2)
	355.0(6) ^b	13(1)			
	381.7(6) ^b	8(1)			
	408.2(6) ^b	12(1)			
	487.9(6)	14(1)	(15/2 ⁻)	(11/2 ⁻)	(E2)
	500.1(6) ^b	4(1)			
	507.1(6) ^b	21(2)			
	520.0(6) ^b	31(1)			
	536.7(6)	9(1)	(15/2 ⁻)	(13/2 ⁻)	(M1 + E2)
	564.4(6)	100(4)	(13/2 ⁻)	9/2 ⁻	(E2)
	598.2(6) ^b	11(4)			
	612.8(6)	32(2)	(11/2 ⁻)	9/2 ⁻	(M1 + E2)
	632.8(6)	33(2)	(17/2 ⁻)	(13/2 ⁻)	(E2)
	638.2(6)	32(2)	(21/2 ⁻)	(17/2 ⁻)	(E2)
	698.7(6) ^b	17(1)			
723.9(6) ^b	5(1)				
737.2(6)	58(4)	(17/2 ⁻)	(13/2 ⁻)	(E2)	
743.1(7)	5(1)	(21/2 ⁻)	(17/2 ⁻)	(E2)	
^{210}Ac	476.1(6)	100(6)			
	834.6(6)	80(7)			

TABLE II. (Continued.)

Nucleus	E_γ (keV)	$I_\gamma^{rel.}$ (%)	I_1^π	I_f^π	σL	
^{211}Ra	146.4(6)	15(1)	(19/2 ⁻)	(17/2 ⁺)	(E1)	
	161.4(6)	7(1)	(15/2 ⁻)	(13/2 ⁻)	(M1 + E2)	
	196.2(7) ^b	9(3)				
	252.5(7) ^b	17(4)				
	263.6(6)	24(2)				
	395.4(2) ^c			(13/2 ⁺)	(9/2 ⁻)	(M2)
	439.3(6)	48(4)		(15/2 ⁻)	(11/2 ⁻)	(E2)
	462.5(7) ^b	11(2)				
	514.7(6)	56(4)			(15/2 ⁻)	
	526.0(6)	54(6)		(17/2 ⁺)	(13/2 ⁺)	(E2)
	531.2(6)	69(6)		(7/2 ⁻)	5/2 ⁻	(M1 + E2)
	601.4(6)	100(8)		(15/2 ⁻)	(13/2 ⁺)	(E1)
	671.9(6)	16(2)		(21/2 ⁺)	(17/2 ⁺)	(E2)
	791.1(6)	39(3)			(15/2 ⁻)	
	800.3(6) ^d	71(4)		(9/2 ⁻)	5/2 ⁻	(E2)
	825.8(6)	49(3)		(11/2 ⁻)	(7/2 ⁻)	(E2)
834.1(6)	22(3)		(13/2 ⁻)	(9/2 ⁻)	(E2)	
873.7(6) ^b	16(2)					

^aEnergy taken from Ref. [9].

^bCould not be placed in the level scheme with confidence.

^cEnergy measured at the focal plane.

^dEnergy measured at the focal plane was 801.5(2) keV.

The half-life of ^{211}Ac was determined again from the recoil- α correlations, using the logarithmic time-scale method [26]. The obtained half-life, 228(4) ms, is in an agreement with the literature value of 210(30) ms [30].

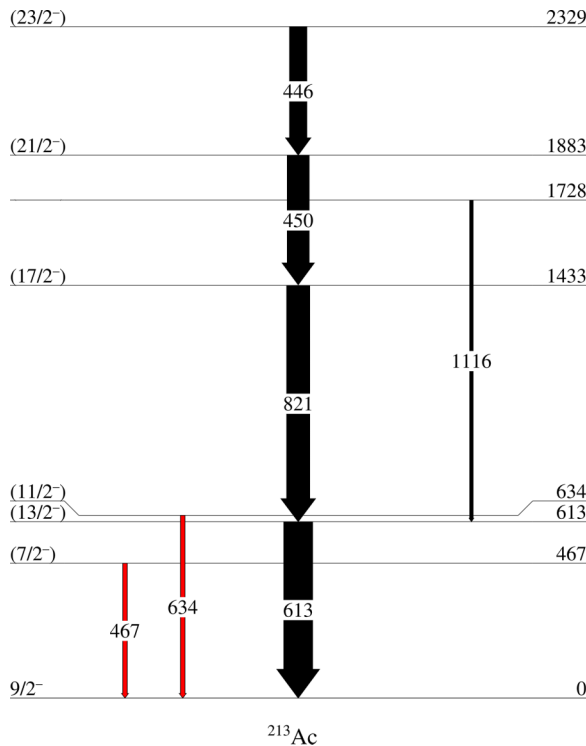


FIG. 5. The proposed level scheme for ^{213}Ac . Transitions in red are from the α -decay work of Ref. [9].

D. Isotope ^{210}Ac

A small concentration of events was observed in the side of the main ^{211}Ac group of the recoil-gated decay-decay

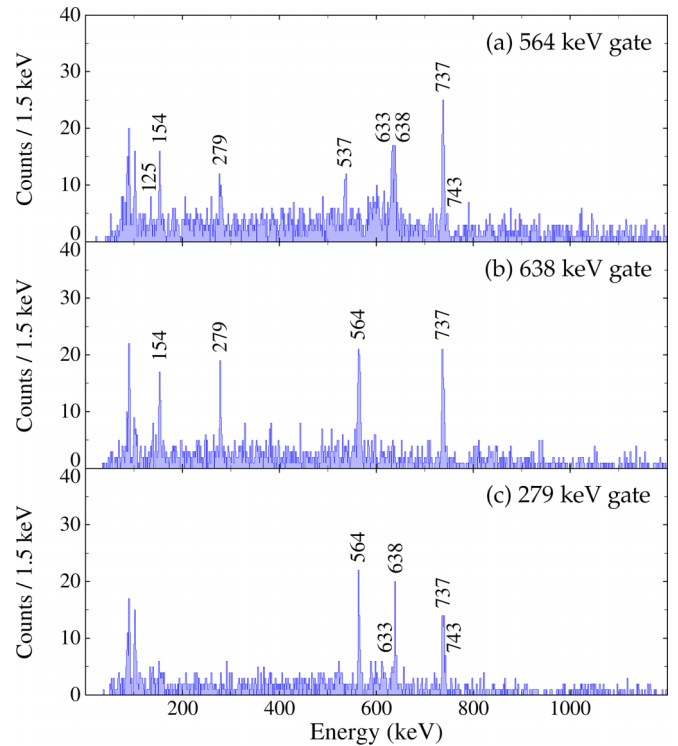


FIG. 6. ^{211}Ac α -decay tagged prompt coincidence γ -ray energy spectra gated on the (a) 564-keV, (b) 638-keV, and (c) 279-keV γ -ray transitions.

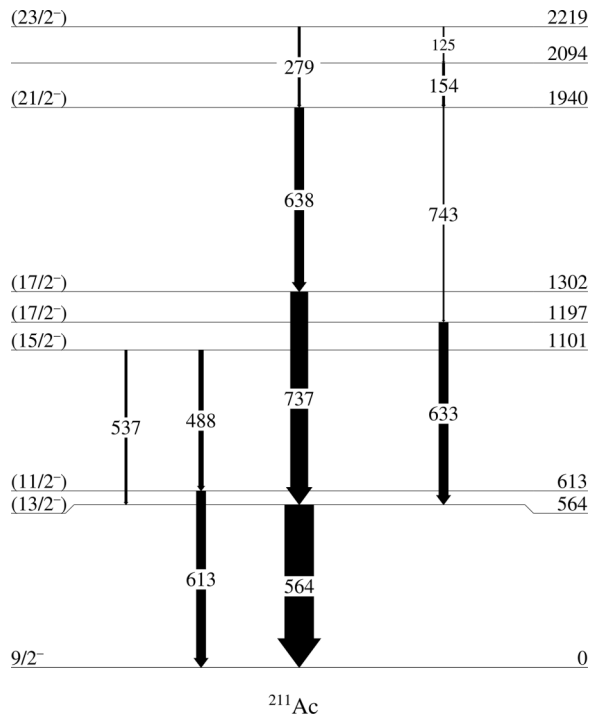


FIG. 7. The proposed level scheme for ^{211}Ac , as deduced from the present data.

matrix. The α -particle energies and decay times of this group match the neighboring isotope ^{210}Ac and its daughter nuclei ^{206}Fr . The application of a stringent recoil- α - α gate to this group brought up the prompt γ -ray energy spectrum shown in Fig. 4(d). Two candidate transitions at energies of 476 keV and 835 keV are clearly distinguished from the ^{211}Ac residual background, and those were then assigned to ^{210}Ac . Properties of these transitions are listed in Table II.

E. Isotope ^{211}Ra

A byproduct of the reaction $^{40}\text{Ar} + ^{175}\text{Lu}$ was the isotope ^{211}Ra , which was produced through the $1p3n$ channel. The 395-keV and 800-keV transitions depopulating the $(^{13/2}^+)$ isomeric state were known prior to this study [15], but we were now able to expand the level scheme considerably. The half-life of the $(^{13/2}^+)$ isomeric state was long enough to be observed at the focal plane. Separate recoil-decay tagging could be made either with the α decays, or with the internal-conversion electrons originating from the 395-keV $M2$ transition that depopulates the isomeric state, see Fig. 8. A delayed γ -ray energy spectrum measured within 50 μs after ^{211}Ra recoil implantation at the focal-plane Ge array is shown in the inset of Fig. 8. The spectrum shows the 395-keV $M2$ transition, 801.5(2)-keV transition [same as the 800.3(6)-keV transition at target position], and x rays from the internal conversion of the 395-keV $M2$ transition. The efficiency corrected intensity ratio of these two transitions agrees well with that reported in Ref. [13].

The internal-conversion electron gated spectrum (red in Fig. 8) clearly shows the transitions at 146, 264, 515, 526, 601, 672, and 791 keV, therefore, they must lie above the isomeric state. Furthermore, the transitions at 439, 531, 800, 826, and 834 keV are completely missing from this spectrum.

These two prompt spectra in Fig. 8, along with the prompt γ - γ coincidences of 826-keV and 834-keV [Figs. 9(a) and 9(b)], and transition energy sums, suggest that there are two decay paths bypassing the $(^{13/2}^+)$ isomeric state. One via the 834-keV transition and the other via the 439-826-531-keV cascade. It is worth of mentioning that the α -decay properties of ^{211}Ra are very similar to those of ^{212}Ra , and the energies of the presently observed 439 and 826-keV transitions are close to those of the $6^+ \rightarrow 4^+$ and $4^+ \rightarrow 2^+$ transitions in ^{212}Ra , respectively. However, contamination from ^{212}Ra is low as indicated by the nonobservation of the ^{212}Ra $2^+ \rightarrow 0^+$

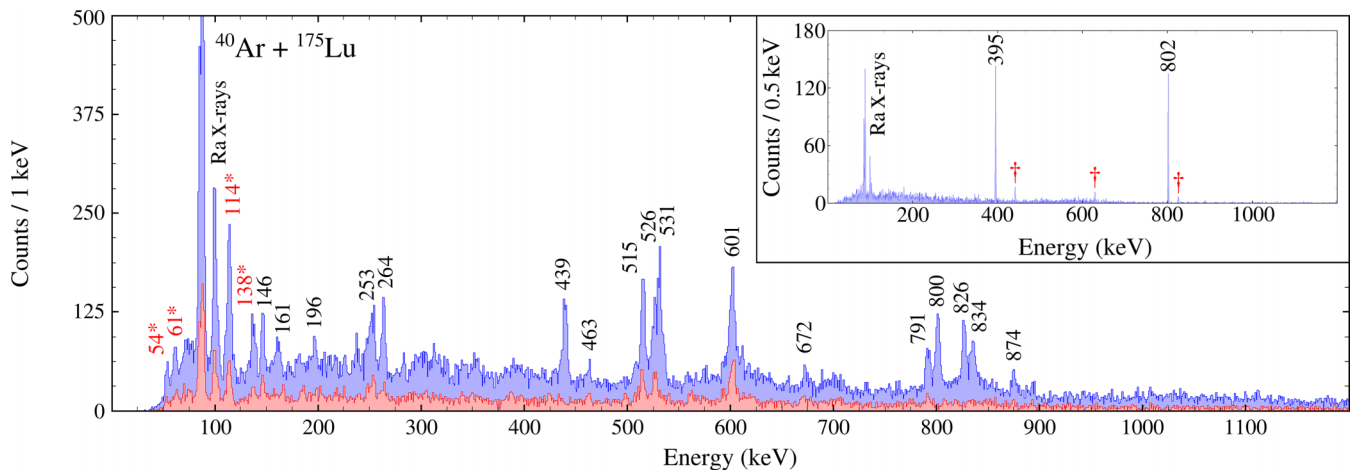


FIG. 8. Two different γ -ray energy spectra for ^{211}Ra from the present study. The blue spectrum was obtained with the gate set on ^{211}Ra α decays, as shown in Fig. 1. The red spectrum was obtained with the gate on the internal conversion electrons, as shown in the bottom left corner in Fig. 1, separating transitions feeding the isomeric $(^{13/2}^+)$ state. The inset shows the α -decay gated delayed transitions of ^{211}Ra observed in the focal-plane Ge-array. Transitions marked in red (*) originate from coulomb excitations of the ^{175}Lu target in the main panel and red (†) in the inset mark transitions of ^{212}Ra .

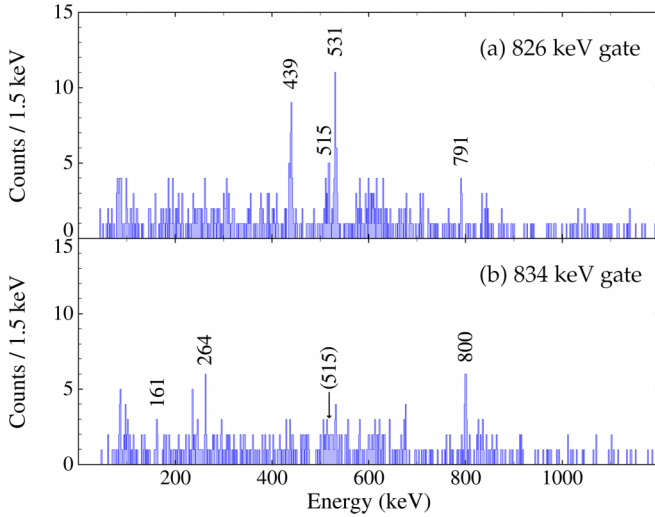


FIG. 9. ^{211}Ra α -decay tagged prompt coincidence γ -ray energy spectra gated on the (a) 826-keV and (b) 834-keV γ -ray transitions.

transition at the energy of 629 keV in the α -decay tagged prompt γ -ray energy spectrum shown in blue in Fig. 8. The proposed level scheme for ^{211}Ra is presented in Fig. 10, and a summary of the observed transitions can be found in Table II.

The half-life of the ground state of ^{211}Ra was determined from the recoil- α correlations, using the logarithmic

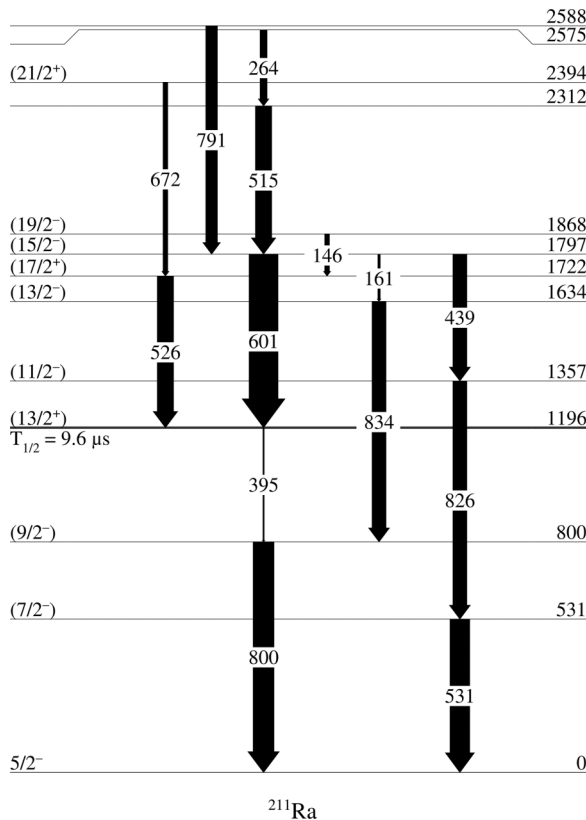


FIG. 10. Proposed level scheme for ^{211}Ra . Intensity of the delayed 395-keV transition is not to scale.

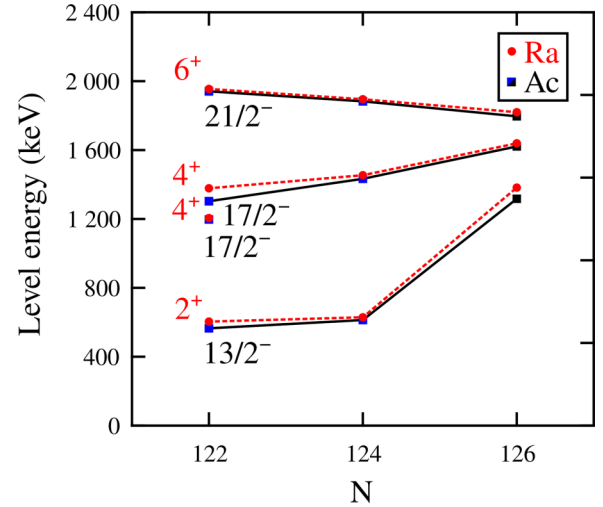


FIG. 11. Level-energy systematics of selected negative-parity states in odd-mass actinium isotopes, compared to positive-parity states in even-even radium isotopes (circles). The blue squares are from the present study, other points are taken from Refs. [36–39].

time-scale method [26]. The obtained result was 13.7(2) s, which is in a good agreement with the literature value of 13(2) s [30]. Additionally, the internal conversion electron correlations were used to obtain a half-life of 9.6(2) μs for the ($^{13}_2$) isomeric state by applying the semilogarithmic scale linear least-square fit method. This is also in a good agreement with the two latest values of 9.7(6) μs reported in Ref. [15] and 9.4(5) μs reported in Ref. [31].

IV. DISCUSSION

In nearby odd- A astatine and francium isotopes it has been observed that the low-lying negative parity yrast states follow the systematics of their respective even-even isotones, see, for example Refs. [32–35] and references therein. This phenomenon can be interpreted as the nucleus having an even-even core and a weakly coupled “spectator” nucleon. The resulting energies of the yrast states are almost the same as those in the core nucleus, but the angular momentum of the odd nucleon is added.

Similarly, the level energies of the ($^{13}_2$), ($^{17}_2$), and ($^{21}_2$) yrast states in odd-even ^{213}Ac and ^{211}Ac follow the energies of the 2^+ , 4^+ , and 6^+ states of their even-even radium core as illustrated in Fig. 11. The energies of these radium equivalent states in the actinium isotopes are a bit lower, but no sudden changes that could indicate a shape or configuration change were observed as expected. The majority of the states in the ^{213}Ac and ^{211}Ac are therefore interpreted arising from the weak coupling of the odd $h_{9/2}$ quasiproton to the associated even-even core states. Spins and parities for the other states are suggested based on the systematics of the lighter odd-even isotones.

In Table III, suggested dominant configurations of the observed states are given. They are based on similarities with the francium isotones and assignments in Refs. [29,40]. While the ($^{21}_2$) states in ^{213}Ac and ^{211}Ac still represent a coupling

TABLE III. Configurations proposed to $^{213,211}\text{Ac}$ and ^{211}Ra .

Nucleus	E_{level} (keV)	I^π	Configuration
^{213}Ac	0	$9/2^-$	$\pi(h_{9/2}) \otimes ^{212}\text{Ra}; 0^+\rangle$
	467	$(7/2^-)$	$\pi(f_{7/2}) \otimes ^{212}\text{Ra}; 0^+\rangle$ or $\pi(h_{9/2}) \otimes ^{212}\text{Ra}; 2^+\rangle$
	613	$(13/2^-)$	$\pi(h_{9/2}) \otimes ^{212}\text{Ra}; 2^+\rangle$
	634	$(11/2^-)$	$\pi(h_{9/2}) \otimes ^{212}\text{Ra}; 2^+\rangle$
	1433	$(17/2^-)$	$\pi(h_{9/2}) \otimes ^{212}\text{Ra}; 4^+\rangle$
	1883	$(21/2^-)$	$\pi(h_{9/2}) \otimes ^{212}\text{Ra}; 6^+\rangle$
	2329	$(23/2^-)$	$\pi(h_{9/2}^2 f_{7/2})$
^{211}Ac	0	$9/2^-$	$\pi(h_{9/2}) \otimes ^{210}\text{Ra}; 0^+\rangle$
	564	$(13/2^-)$	$\pi(h_{9/2}) \otimes ^{210}\text{Ra}; 2^+\rangle$
	613	$(11/2^-)$	$\pi(h_{9/2}) \otimes ^{210}\text{Ra}; 2^+\rangle$
	1101	$(15/2^-)$	$\pi(h_{9/2}) \otimes ^{210}\text{Ra}; 4^+\rangle$
	1197	$(17/2^-)$	$\pi(h_{9/2}) \otimes ^{210}\text{Ra}; 4^+\rangle$
	1302	$(17/2^-)$	$\pi(h_{9/2}) \otimes ^{210}\text{Ra}; 4^+\rangle$
	1940	$(21/2^-)$	$\pi(h_{9/2}) \otimes ^{210}\text{Ra}; 6^+\rangle$
	2219	$(23/2^-)$	$\pi(h_{9/2}^2 f_{7/2})$
^{211}Ra	0	$5/2^-$	$\nu(f_{5/2}^{-1}) \otimes ^{212}\text{Ra}; 0^+\rangle$
	531	$(7/2^-)$	$\nu(f_{5/2}^{-1}) \otimes ^{212}\text{Ra}; 2^+\rangle$
	800	$(9/2^-)$	$\nu(f_{5/2}^{-1}) \otimes ^{212}\text{Ra}; 2^+\rangle$
	1196	$(13/2^+)$	$\nu(i_{13/2}^{-1}) \otimes ^{212}\text{Ra}; 0^+\rangle$
	1357	$(11/2^-)$	$\nu(f_{5/2}^{-1}) \otimes ^{212}\text{Ra}; 4^+\rangle$
	1634	$(13/2^-)$	$\nu(f_{5/2}^{-1}) \otimes ^{212}\text{Ra}; 4^+\rangle$
	1722	$(17/2^+)$	$\nu(i_{13/2}^{-1}) \otimes ^{212}\text{Ra}; 2^+\rangle$
	1797	$(15/2^-)$	$\nu(f_{5/2}^{-1}) \otimes ^{212}\text{Ra}; 6^+\rangle$
	1868	$(19/2^-)$	$\nu(f_{5/2}^{-1}) \otimes ^{212}\text{Ra}; 8^+\rangle$
	2394	$(21/2^+)$	$\nu(i_{13/2}^{-1}) \otimes ^{212}\text{Ra}; 4^+\rangle$

of the $h_{9/2}$ quasiproton to the rather pure 6^+ member of the proton $h_{9/2}^6$ seniority multiplet of the radium core, opening of the $N = 126$ closed shell generates several 4^+ and especially 2^+ states with mixed configurations seen as a sudden drop of energies of the low-lying yrast states in these nuclei. In ^{212}Ra , the 2^+ state can be associated with a dominant neutron $(p_{1/2}^{-1} f_{5/2}^{-1})_{2^+}$ configuration and in ^{210}Ra with a dominant neutron $(p_{1/2}^{-2} f_{5/2}^{-2})_{2^+}$ configuration [36,37].

Similarly to ^{209}Fr , we observe two $(\frac{17}{2}^-)$ states in ^{211}Ac , the upper one being favored in the de-excitation of the $(\frac{21}{2}^-)$ state by $E2$ transitions. Therefore, as in ^{209}Fr , it is assigned with a coupling of the $h_{9/2}$ quasiproton to the 4_2^+ core state of the dominant proton $h_{9/2}^6$ configuration. The lower (yrast) $(\frac{17}{2}^-)$ state represents a coupling of the same proton to a 4_1^+ state of a dominant neutron $(p_{1/2}^{-2} f_{5/2}^{-2})_{4^+}$ configuration. Such 4^+ states with similar assignments have been observed in ^{210}Ra [37].

The case of the even-odd ^{211}Ra is similar to that of ^{211}Ac and ^{213}Ac , but instead of the extra proton, it has an active neutron-hole in the $f_{5/2}$ shell. Its structure therefore resembles that of its heavier neighboring even-even isotope ^{212}Ra . Consequently, the level energy systematics of $N = 123$ isotones exhibit smooth behavior, as shown in Fig. 12. The list of

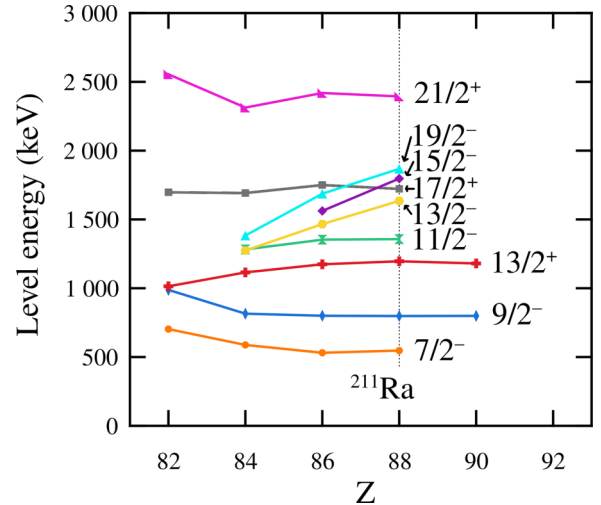


FIG. 12. Level-energy systematics of selected states in $N = 123$ isotones. The points on the dotted line ($Z = 88$) are the proposed levels in ^{211}Ra from the present study. The other points are taken from Refs. [42–45].

suggested configurations for observed states of ^{211}Ra can be found in Table III.

Both ^{212}Ra and ^{210}Ra have a low-lying isomeric 8^+ state with a half-life of several microseconds, but no signs of such metastable states were seen in ^{213}Ac nor in ^{211}Ac . However, nuclei in this area of the nuclear chart are known to have isomeric states with half-lives around 10–100 ns. For example, in nearby astatine and francium nuclei, isomeric states with a spin and parity of $\frac{25}{2}^+$ or $\frac{29}{2}^+$ are commonly present [29,32,33,40,41]. Our setup was not sensitive to decays of isomeric states within this time regime as they would predominantly decay in flight, outside both the target and focal-plane positions, and thus would remain unnoticed. The time of flight through the separator was close to 1.3 μs . The presence of such nanosecond-scale isomers might explain the sudden termination of the observed cascades above the $(\frac{23}{2}^-)$ state. Furthermore, the strong internal conversion branches and resulting strong x-ray background, could also prevent us from observing low-energy transitions, also abundant in nearby nuclei. The level structure of nearby nuclei fragments above the $\frac{21}{2}^-$ state, which makes it difficult to construct level schemes, especially with limited statistics.

However, the recoil-decay tagging method is one of the few feasible ways to probe the excited states of actinium isotopes. A clean tag is needed for unambiguous identification of reaction products as the nuclei in this region share remarkably similar decay properties. The power of combining an in-flight separator with the RDT method lies on the unprecedented selectivity gained from the multiple tagging conditions at the focal plane. When employed with an efficient Ge-detector array at the target area, it enables a clean identification of cascades of prompt γ -ray transitions, including those bypassing isomers. Moreover, the observed intensities of prompt γ rays allow the order of transitions in a cascade to be determined, which is difficult in off-beam detection of γ rays emitted in

TABLE IV. Summary of the measured half-lives ($T_{\frac{1}{2}}^{\text{meas.}}$) together with the values from literature ($T_{\frac{1}{2}}^{\text{lit.}}$).

Nucleus	$T_{\frac{1}{2}}^{\text{meas.}}$	$T_{\frac{1}{2}}^{\text{lit.}}$
^{211}Ra	13.7(2) s	13(2) s [30]
$^{211\text{m}}\text{Ra}$	9.6(2) μs	9.7(6) μs [15]
^{211}Ac	228(4) ms	210(30) ms [30]
^{212}Ac	881(15) ms	880(35) ms [28]
^{213}Ac	771(14) ms	738(16) ms [27]

the decay of isomers. For these reasons the low-lying level structure of many radium, francium, and astatine isotopes in this region are not without ambiguities and could certainly benefit from further studies using in-beam RDT methods to, for example, probe de-excitation paths bypassing the 8^+ and other isomeric states.

V. SUMMARY

In the present work, we have established the first level scheme for the isotope ^{211}Ac , corrected and extended the level scheme for the isotope ^{213}Ac . We have shown that the energies of their ($\frac{13}{2}^-$), ($\frac{17}{2}^-$), ($\frac{21}{2}^-$) states closely follow the energies of their respective even-even core states in a similar manner as has been seen in the other odd-even nuclei in this region. γ -ray

transitions assigned to the odd-odd ^{210}Ac and ^{212}Ac isotopes were identified but no level scheme was constructed. We also extended the level scheme of even-odd isotope ^{211}Ra beyond the ($\frac{13}{2}^+$) isomeric state, and identified two parallel decay paths bypassing the metastable state. This enabled us to assign configurations and extend systematics of high-spin states of $N = 123$ isotones up to $Z = 88$. Additionally, we measured the half-lives for all isotopes and isomeric states present in the data, for which an improvement could be made. These values are summarized in Table IV.

The data obtained in the present work and the corresponding metadata are available online [46].

ACKNOWLEDGMENTS

This work was supported by the Research Council of Finland under Contracts No. 323710, No. 347154, No. 353786 (personal research projects, KA), and No. 339245. The project has received funding from the EU Horizon 2020 research and innovation programme under Grant Agreement No. 861198–LISA–H2020–MSCA–ITN–2019. The authors thank the GAMMAPOOL European Spectroscopy Resource for the loan of the germanium detectors and GSI target laboratory for providing the carbon foils and targets for this experiment. The authors would also like to express their gratitude to the technical staff of the Accelerator Laboratory at the University of Jyväskylä for their support.

- [1] R. Julin, T. Grahn, J. Pakarinen, and P. Rahkila, *J. Phys. G: Nucl. Part. Phys.* **43**, 024004 (2016).
- [2] C. Qi, R. Liotta, and R. Wyss, *Prog. Part. Nucl. Phys.* **105**, 214 (2019).
- [3] R. Ferrer, A. Barzakh, B. Bastin, R. Beerwerth, M. Block, P. Creemers, H. Grawe, R. de Groote, P. Delahaye, X. Fléchéard, S. Franchoo, S. Fritzsche, L. P. Gaffney, L. Ghys, W. Gins, C. Granados, R. Heinke, L. Hijazi, M. Huyse, T. Kron *et al.*, *Nat. Commun.* **8**, 14520 (2017).
- [4] J. Ojala, J. Pakarinen, P. Papadakis, J. Sorri, M. Sandzelius, D. M. Cox, K. Auranen, H. Badran, P. J. Davies, T. Grahn, P. T. Greenlees, J. Henderson, A. Herzán, R.-D. Herzberg, J. Hilton, U. Jakobsson, D. G. Jenkins, D. T. Joss, R. Julin, S. Juutinen *et al.*, *Commun. Phys.* **5**, 213 (2022).
- [5] S. Hilaire and M. Girod, *Eur. Phys. J. A* **33**, 237 (2007).
- [6] P. Möller, A. Sierk, T. Ichikawa, and H. Sagawa, *At. Data Nucl. Data Tables* **109–110**, 1 (2016).
- [7] M. Leino, J. Uusitalo, T. Enqvist, K. Eskola, A. Jokinen, K. Loberg, W. H. Trzaska, and J. Äystö, *Z. Phys. A* **348**, 151 (1994).
- [8] F. P. Heßberger, S. Hofmann, D. Ackermann, V. Ninov, M. Leino, S. Saro, A. Andreyev, A. Lavrentev, A. G. Popeko, and A. V. Yeremin, *Eur. Phys. J. A* **8**, 521 (2000).
- [9] F. Heßberger, S. Hofmann, I. Kojouharov, D. Ackermann, S. Antalic, P. Čagarda, B. Kindler, B. Lommel, R. Mann, A. Popeko, S. Saro, J. Uusitalo, and A. Yeremin, *Eur. Phys. J. A* **15**, 335 (2002).
- [10] Z. Y. Zhang, Z. G. Gan, L. Ma, L. Yu, H. B. Yang, T. H. Huang, G. S. Li, Y. L. Tian, Y. S. Wang, X. X. Xu, X. L. Wu, M. H. Huang, C. Luo, Z. Z. Ren, S. G. Zhou, X. H. Zhou, H. S. Xu, and G. Q. Xiao, *Phys. Rev. C* **89**, 014308 (2014).
- [11] J. Wang, Z. Gan, Z. Zhang, M. Huang, L. Ma, M. Zhang, H. Yang, C. Yang, Y. Qiang, X. Huang, Z. Zhao, S. Xu, Z. Li, L. Chen, L. Sun, H. Zhou, X. Zhang, X. Wu, Y. Tian, Y. Wang *et al.*, *Phys. Lett. B* **850**, 138503 (2024).
- [12] C. Granados, P. Creemers, R. Ferrer, L. P. Gaffney, W. Gins, R. de Groote, M. Huyse, Y. Kudryavtsev, Y. Martínez, S. Raeder, S. Sels, C. Van Beveren, P. Van den Bergh, P. Van Duppen, K. Wrzosek-Lipska, A. Zadornaya, A. E. Barzakh, B. Bastin, P. Delahaye, L. Hijazi *et al.*, *Phys. Rev. C* **96**, 054331 (2017).
- [13] F. P. Heßberger, S. Hofmann, I. Kojouharov, and D. Ackermann, *Eur. Phys. J. A* **22**, 253 (2004).
- [14] P. Kuusiniemi, F. P. Heßberger, D. Ackermann, S. Hofmann, B. Sulignano, I. Kojouharov, and R. Mann, *Eur. Phys. J. A* **25**, 397 (2005).
- [15] K. Hauschild, A. Yeremin, O. Dorvaux, A. Lopez-Martens, A. Belozero, C. Briancón, M. Chelnokov, V. Chepigin, S. Garcia-Santamaria, V. Gorshkov, F. Hanappe, A. Kabachenko, A. Korichi, O. Malyshev, Y. Oganessian, A. Popeko, N. Rowley, A. Shutov, L. Stuttgé, and A. Svirikhin, *Nucl. Instrum. Methods Phys. Res. A* **560**, 388 (2006).
- [16] J. Pakarinen, J. Ojala, P. Ruotsalainen, H. Tann, H. Badran, T. Calverley, J. Hilton, T. Grahn, P. T. Greenlees, M. Hytönen, A. Illana, A. Kauppinen, M. Luoma, P. Papadakis, J. Partanen, K. Porras, M. Puskala, P. Rahkila, K. Ranttila, J. Sarén *et al.*, *Eur. Phys. J. A* **56**, 149 (2020).
- [17] J. Sarén, J. Uusitalo, M. Leino, P. Greenlees, U. Jakobsson, P. Jones, R. Julin, S. Juutinen, S. Ketelhut, M. Nyman, P. Peura,

- and P. Rahkila, *Nucl. Instrum. Methods Phys. Res. B* **266**, 4196 (2008).
- [18] J. Uusitalo, J. Sarén, J. Partanen, and J. Hilton, *Acta Phys. Pol. B* **50**, 319 (2019).
- [19] E. S. Paul, P. J. Woods, T. Davinson, R. D. Page, P. J. Sellin, C. W. Beausang, R. M. Clark, R. A. Cunningham, S. A. Forbes, D. B. Fossan, A. Gizon, J. Gizon, K. Hauschild, I. M. Hibbert, A. N. James, D. R. LaFosse, I. Lazarus, H. Schnare, J. Simpson, R. Wadsworth *et al.*, *Phys. Rev. C* **51**, 78 (1995).
- [20] R. S. Simon, K. H. Schmidt, F. P. Heßberger, S. Hlavac, M. Honusek, G. Münzenberg, H. G. Clerc, U. Gollerthan, and W. Schwab, *Z. Phys. A* **325**, 197 (1986).
- [21] I. Lazarus, E. Appelbe, P. Butler, P. Coleman-Smith, J. Cresswell, S. Freeman, R. Herzberg, I. Hibbert, D. Joss, S. Letts, R. Page, V. Pucknell, P. Regan, J. Sampson, J. Simpson, J. Thornhill, and R. Wadsworth, *IEEE Trans. Nucl. Sci.* **48**, 567 (2001).
- [22] J. Sarén, J. Uusitalo, and H. Joukainen, *Nucl. Instrum. Methods Phys. Res. B* **541**, 33 (2023).
- [23] M. Martin, *Nucl. Data Sheets* **108**, 1583 (2007).
- [24] J. Chen and F. Kondev, *Nucl. Data Sheets* **126**, 373 (2015).
- [25] P. Kuusiniemi, F. P. Heßberger, D. Ackermann, S. Hofmann, and I. Kojouharov, *Eur. Phys. J. A* **22**, 429 (2004).
- [26] K. H. Schmidt, *Eur. Phys. J. A* **8**, 141 (2000).
- [27] M. Basunia, *Nucl. Data Sheets* **181**, 475 (2022).
- [28] H. Yang, L. Ma, Z. Zhang, L. Yu, G. Jia, M. Huang, Z. Gan, T. Huang, G. Li, X. Wu, Y. Fang, Z. Wang, B. Gao, and W. Hua, *J. Phys. G: Nucl. Part. Phys.* **41**, 105104 (2014).
- [29] G. D. Dracoulis, P. M. Davidson, G. J. Lane, A. P. Byrne, T. Kibédi, P. Nieminen, H. Watanabe, and A. N. Wilson, *Phys. Rev. C* **79**, 054313 (2009).
- [30] B. Singh, D. Abriola, C. Baglin, V. Demetriou, T. Johnson, E. McCutchan, G. Mukherjee, S. Singh, A. Sonzogni, and J. Tuli, *Nucl. Data Sheets* **114**, 661 (2013).
- [31] A. D. Bacelar, A. Bruce, Z. Podolyák, N. Al-Dahan, M. Górska, S. Lalkovski, S. Pietri, M. Ricciardi, A. Algora, N. Alkhomashi, J. Benlliure, P. Boutachkov, A. Bracco, E. Calore, E. Casarejos, I. Cullen, A. Deo, P. Detistov, Z. Dombradi, C. Domingo-Pardo *et al.*, *Phys. Lett. B* **723**, 302 (2013).
- [32] K. Auranen, J. Uusitalo, S. Juutinen, U. Jakobsson, T. Grahn, P. T. Greenlees, K. Hauschild, A. Herzán, R. Julin, J. Konki, M. Leino, J. Pakarinen, J. Partanen, P. Peura, P. Rahkila, P. Ruotsalainen, M. Sandzelius, J. Sarén, C. Scholey, J. Sorri, and S. Stolze, *Phys. Rev. C* **91**, 024324 (2015).
- [33] K. Auranen, J. Uusitalo, S. Juutinen, H. Badran, F. Defranchi Bisso, D. Cox, T. Grahn, P. T. Greenlees, A. Herzán, U. Jakobsson, R. Julin, J. Konki, M. Leino, A. Lightfoot, M. J. Mallaburn, O. Neuvonen, J. Pakarinen, P. Papadakis, J. Partanen, P. Rahkila *et al.*, *Phys. Rev. C* **97**, 024301 (2018).
- [34] U. Jakobsson, J. Uusitalo, S. Juutinen, M. Leino, T. Enqvist, P. T. Greenlees, K. Hauschild, P. Jones, R. Julin, S. Ketelhut, P. Kuusiniemi, M. Nyman, P. Peura, P. Rahkila, P. Ruotsalainen, J. Sarén, C. Scholey, and J. Sorri, *Phys. Rev. C* **85**, 014309 (2012).
- [35] U. Jakobsson, S. Juutinen, J. Uusitalo, M. Leino, K. Auranen, T. Enqvist, P. T. Greenlees, K. Hauschild, P. Jones, R. Julin, S. Ketelhut, P. Kuusiniemi, M. Nyman, P. Peura, P. Rahkila, P. Ruotsalainen, J. Sarén, C. Scholey, and J. Sorri, *Phys. Rev. C* **87**, 054320 (2013).
- [36] T. Palazzo, G. J. Lane, A. E. Stuchbery, A. J. Mitchell, A. Akber, M. S. M. Gerathy, S. S. Hota, T. Kibédi, B. Q. Lee, N. Palalani, and M. W. Reed, *Phys. Rev. C* **97**, 014323 (2018).
- [37] J. J. Ressler, C. W. Beausang, H. Ai, H. Amro, M. A. Caprio, R. F. Casten, A. A. Hecht, S. D. Langdown, E. A. McCutchan, D. A. Meyer, P. H. Regan, M. J. S. Sciacchitano, A. Yamamoto, and N. V. Zamfir, *Phys. Rev. C* **69**, 034331 (2004).
- [38] D. J. Decman, H. Grawe, H. Kluge, and K. H. Maier, *Z. Phys. A* **310**, 55 (1983).
- [39] A. Stuchbery, G. Dracoulis, T. Kibédi, A. Byrne, B. Fabricius, A. Poletti, G. Lane, and A. Baxter, *Nucl. Phys. A* **548**, 159 (1992).
- [40] A. Byrne, G. Dracoulis, C. Fahlander, H. Hübel, A. Poletti, A. Stuchbery, J. Gerl, R. Davie, and S. Poletti, *Nucl. Phys. A* **448**, 137 (1986).
- [41] K. Yadav, A. Y. Deo, Madhu, D. Sahoo, P. C. Srivastava, S. Suman, S. K. Tandel, A. Sharma, I. Ahmed, K. Katre, K. R. Devi, S. Dutt, S. Kumar, Yashraj, S. Muralithar, and R. P. Singh, *Phys. Rev. C* **107**, 054303 (2023).
- [42] J. Khuyagbaatar, S. Hofmann, F. P. Heßberger, D. Ackermann, S. Antalic, H. G. Burkhard, S. Heinz, B. Kindler, A. F. Lisetskiy, B. Lommel, R. Mann, K. Nishio, H. J. Schött, and B. Sulignano, *Eur. Phys. J. A* **34**, 355 (2007).
- [43] A. Poletti, G. Dracoulis, C. Fahlander, and A. Byrne, *Nucl. Phys. A* **440**, 118 (1985).
- [44] V. Rahkonen, B. Fant, C. Herrlander, K. Honkanen, A. Källberg, and T. Weckström, *Nucl. Phys. A* **441**, 11 (1985).
- [45] J. H. Hamilton, V. Ananthakrishnan, A. V. Ramayya, W. M. LaCasse, D. C. Camp, J. J. Pinajian, L. H. Kern, and J. C. Manthuruthil, *Phys. Rev. C* **6**, 1265 (1972).
- [46] <https://doi.org/10.23729/62121f8e-6d57-46b8-b74c-be32d7672957>